Rare earth effect of yttrium on formation and property of Cr_2O_3 oxide film formed on Co-Cr binary alloy*

JIN Huiming[1]**, FELIX A. Congrado[2] and AROYAVE M. Hayara[2]

(1. College of Mechanical Engineering, Yangzhou University, Yangzhou 225005, China; 2. College of Materials Science and Engineering, National University of Antiuquia, Medellin 23715, Colombia)

Received April 5, 2005; revised June 8, 2005

Abstract The isothermal oxidizing kinetics of Co-40Cr alloy and its yttrium ion-implanted samples were studied at 1000 ℃ in air by thermal-gravity analysis (TGA). Scanning electronic microscopy (SEM) was used to examine the Cr_2O_3 oxide film's morphology after oxidation. Secondary ion mass spectrum (SIMS) method was used to examine the binding energy change of chromium caused by Y-doping and its influence on formation of Cr_2O_3 film. Acoustic emission (AE) method was used *in situ* to monitor the cracking and spalling of oxide films formed on both samples during oxidizing and subsequent air-cooling stages. Theoretical model simulating the film fracture process was proposed to analyze the acoustic emission spectrum both on time domain and on AE-event number domain. It is found that yttrium ion-implantation can remarkably reduce the isothermal oxidizing rate of Co-40Cr and improve the anti-cracking and anti-spalling properties of Cr_2O_3 oxide film. Reasons for the improvement are mainly that the implanted yttrium can reduce the grain size of Cr_2O_3 oxide, increase the high temperature plasticity of oxide film, and remarkably reduce the number and size of Cr_2O_3/Co-40Cr interfacial defects.

Keywords: **interface, binding energy, acoustic emission, oxidation, yttrium.**

The resistance of high temperature alloys to oxidizing environment depends on the formation of slowly growing and adherent oxide films. Usually there are intrinsic growing stress and external thermal stress formed in oxide films[1,2]. The former might arise from the volume changes when the metal is oxidized to oxide, while the latter might arise from the thermal expansion difference between the metal and the oxides. Many studies[1—8] related to the isothermal and cyclic oxidation behaviors of different super-alloys and high temperature coatings have been carried out, and several methods have been developed to measure the residual stresses inside the oxide films, because the residual stress level may be one critical factor influencing the cracking and spalling of oxide films. In this paper, acoustic emission method is used to monitor the cracking and spalling of oxide film formed on Co-40Cr alloy during high temperature oxidation, related mechanical and mathematical model is proposed to study the Cr_2O_3/Co-40Cr interfacial defects' distribution, and finally the influence of yttrium ion-implantation on the high temperature oxidation of Co-40Cr is evaluated by this acoustic emission method and other oxide structure analytical methods.

1 Experiment

Co-40Cr alloy was wire-cut into 10 mm × 10 mm × 1 mm samples which were ultimately polished by 0.2 μm Al_2O_3 abrasive paste. After being ultrasonically cleaned in acetone and alcohol, some specimens were treated by yttrium ion-implantation with 3×10^{17} Y^+/cm^2 using MEVVE-8010 ion-implantation machine. Isothermal oxidation experiment was carried out at 1000 ℃ in air in M25DV thermal balance to study the oxidation kinetics of Co-40Cr and Y-implanted Co-40Cr alloy. In acoustic emission (AE) experiment, Y-free and Y-containing specimens were point-welded to platinum wave-guides (2 mm in diameter) which were connected to AE-100 acoustic emission apparatus. The schematic diagram of the AE experiment is shown in Fig. 1.

These specimens were isothermally oxidized at 1000 ℃ in air for 90 h and then air-cooled to room temperature. During the whole process acoustic emission (AE) signals were monitored *in situ* using the AE-100 unit with the threshold voltage of 84 dB.

Scanning electronic microscopy (SEM) was used to examine the surface morphologies of oxide films

* Supported by National Natural Science Foundation of China (Grant No. 29231011)

** To whom correspondence should be addressed. E-mail: doctorjhm@sohu.com

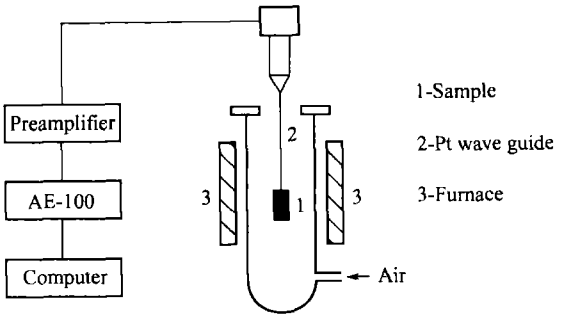

Fig. 1. Schematic diagram of acoustic emission experiment.

formed on Co-40Cr alloys with and without yttrium. Secondary ion mass spectrum (SIMS) technique was used to analyze the yttrium depth profile in substrate Co-40Cr before oxidation and in Cr_2O_3 oxide film after oxidation, and was also used to measure the binding energy changes of element Cr caused by yttrium ion-implantation.

2 Results

The isothermal oxidation mass-gain curves of Co-40Cr and Y-implanted Co-40Cr are shown in Fig. 2. It can be seen that yttrium ion-implantation greatly reduces the oxidizing rate of Co-40Cr alloy.

Fig. 3 is the SEM morphology of the oxide films formed on Co-40Cr and its Y-implanted samples after 24 h isothermal oxidation. It can be found that yttrium ion-implantation remarkably reduces the grain size of oxide film, and the ridge characteristic has apparently arisen in the Y-containing oxide film. Energy dispersive spectrum (EDS) analysis shows that oxide films formed on Co-40Cr with and without yttrium are both pure Cr_2O_3, which is due to the high Cr content and its preferential oxidation in the Co-Cr binary system.

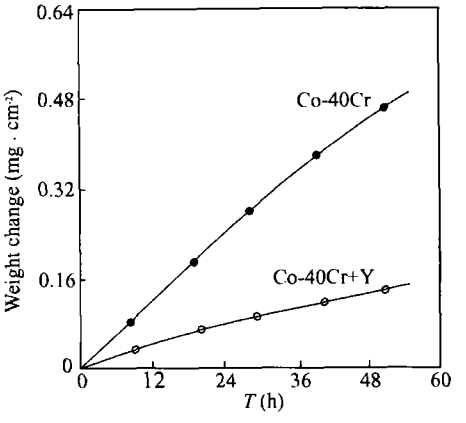

Fig. 2. Isothermal oxidizing mass gain curves of Co-40Cr and Y-implanted Co-40Cr.

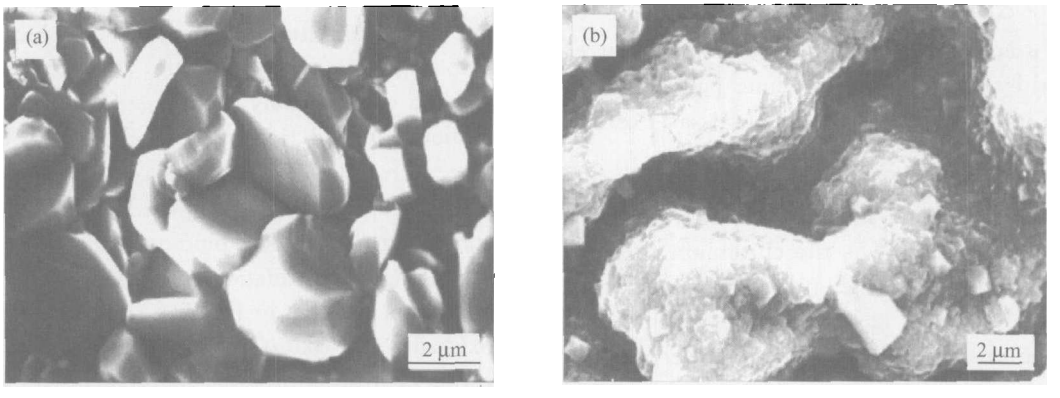

Fig. 3. SEM morphologies of oxide films formed on (a) Co-40Cr and (b) Y-implanted Co-40Cr after 24 h isothermal oxidation.

In acoustic emission experiment, almost no AE signal was detected during the 90 h isothermal oxidizing stage, while at the air-cooling stage many AE signals were detected as shown in Fig. 4. Usually there are internal growth stress σ_{gw} and external thermal stress σ_{th} accumulated in oxide films. When the accumulated stress reached a critical level, it might be released by high temperature creeping of oxide film or by cracking and spalling of oxide film. The former method for stress release occurs slowly and cannot create AE signals, while the latter occurs transiently and can create detectable AE signals. From Fig. 4, we can see that Cr_2O_3 oxide film formed on Co-40Cr begins cracking and spalling when temperature drops to about 910 ℃, while Cr_2O_3 film formed on Co-40Cr with yttrium begins cracking and spalling at about 570 ℃. This illustrated that Cr_2O_3 oxide film formed on Y-implanted Co-40Cr has better property of anti-thermal shocking than its Y-free counterpart.

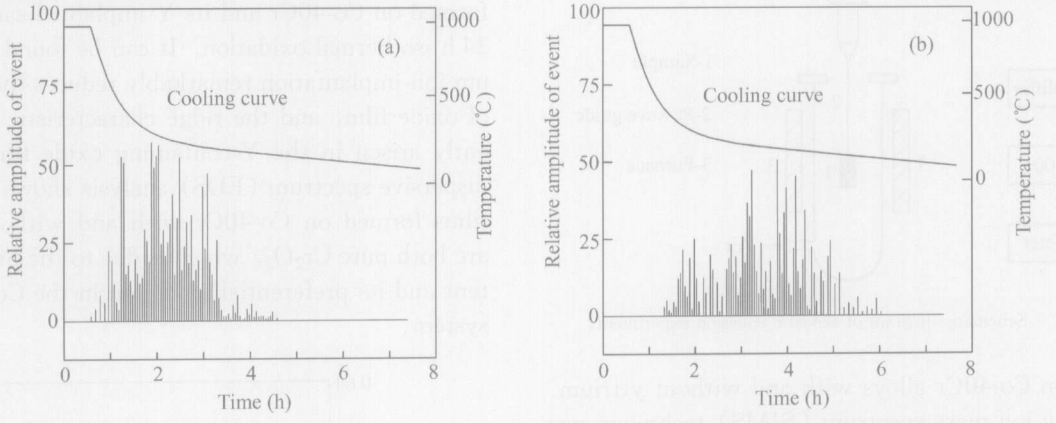

Fig. 4. AE signal distributions measured at the air-cooling stage after 90 h isothermal oxidation of (a) Co-40Cr and (b) Y-implanted Co-40Cr.

In secondary ion mass spectrum (SIMS) experiment, the accelerating energy of first Ar^+ ion was 15 keV, the ionic intensity was 0.5 μA and the diameter of the first ion beam was 80 μm. When the sample surface was bombarded by the first Ar^+ ion, the kinetic energy of the first Ar^+ ion (E_P) was equal to the total kinetic energy of the secondary ion (E_K), element binding energy (E_B) and energy loss (E_L). During the experiment, E_P was kept at a constant value and E_L could be regarded as unchangeable, so the binding energy change for an element is

$$\Delta E_B = -\Delta E_K = -e\Delta U_R, \qquad (1)$$

where ΔU_R is the retarding voltage change that can be obtained by extrapolating the liner part of the secondary ion intensity curves to U_R abscissa (Fig. 5).

Fig. 5(a) is the chromium secondary ion intensity curve of Y-free and Y-implanted Co-40Cr before oxidation, and Fig. 5(b) is the chromium secondary ion intensity curve of the two samples after 1 h isothermal oxidation. Fig. 5(c) is the yttrium depth profile along the oxide/substrate cross section after 10 h isothermal oxidation, in which the position of the oxide/alloy interface was determined by detecting the secondary Co^{2+} ion intensity changes during the Ar^+ sputtering process. From Fig. 5(c) we can find that after long time oxidation the implanted yttrium exists mainly on the outer side of the Cr_2O_3 film.

3 Discussion

By comparing the two oxidizing kinetic curves in Fig. 2, we can find that yttrium ion-implantation remarkably reduces the isothermal oxidizing rate of Co-40Cr. Meanwhile, yttrium ion-implantation can greatly refine the grain size of Cr_2O_3 and promote ridge formation within the oxide film in Fig. 4(b).

Usually the maximum depth of yttrium ion-implantation is less than 100 nm and it will introduce large amounts of dislocations in alloy surface[3]. During the initial oxidizing stage (this time interval might be as short as several seconds), the implanted yttrium with high local concentration and high chemical activity can act as the Cr_2O_3 crystal forming site and promote fine-grained Cr_2O_3 oxide formation[2]. In our SIMS experiments, it can be found that yttrium ion-implantation can reduce the Cr binding energy before oxidation (Fig. 5(a)). This effect means that yttrium can probably increase the Cr_2O_3 crystal formation rate and finally refine the Cr_2O_3 oxide grain size[2]. In addition, yttrium can inhibit $[Cr^{3+}]$ ion diffusion within the Cr_2O_3 oxide film, which can be confirmed by the Cr binding energy increase after some long time oxidation (e.g. 1 h of oxidation in our experiment shown in Fig. 5(b)), and can change the oxidizing rate-controlling step from predominant $[Cr^{3+}]$ cation outwards diffusion to predominant $[O^{2-}]$ anion inward diffusion. Studies related to the ionic diffusion within oxide film have been investigated by some researchers[2,7] using O^{16}/O^{18} tracing element experiment. Predominant $[Cr^{3+}]$ cation's outwards diffusion was inhibited. This could partially be confirmed by our SIMS experiment, in which yttrium's final position after 10 h oxidation was located on the outer side of the Cr_2O_3 oxide film, as shown in Fig. 5(c). The actual existing form of implanted yttrium within Cr_2O_3 oxide film is very fine Y_2O_3, $YCrO_3$ spinel particles or even Y^{3+} ions located at Cr_2O_3 grain boundaries[2,3,7].

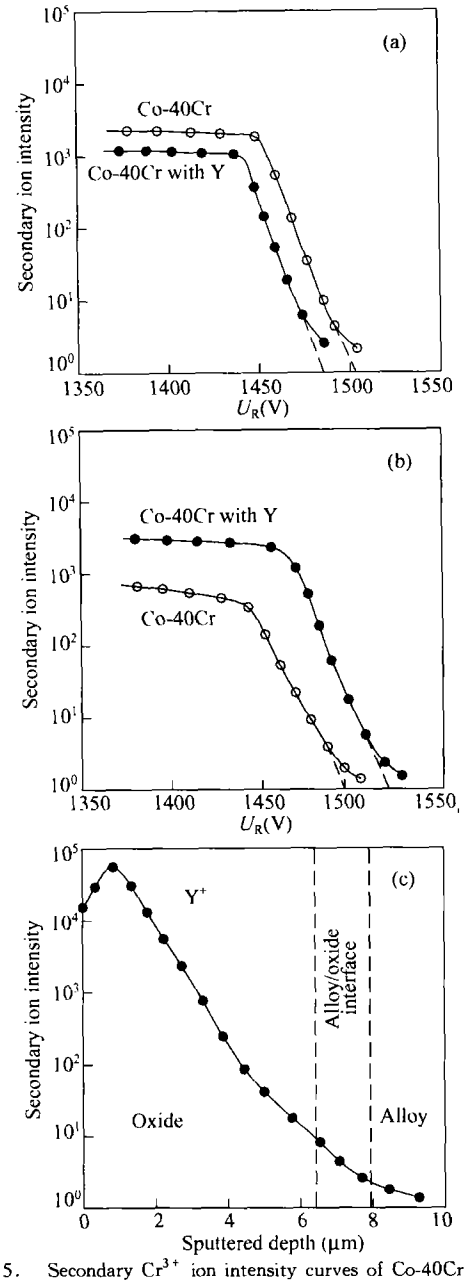

Fig. 5. Secondary Cr^{3+} ion intensity curves of Co-40Cr and Y-implanted Co-40Cr (a) before and (b) after oxidation, and (c) the Y depth profile along the oxide/substrate cross section after 10 h isothermal oxidation.

This kind of fine-grained oxide film has better high temperature plasticity and creeping property, which means that Cr_2O_3 oxide film can release parts of internal compressive stress by means of high temperature creeping rather than by cracking and spalling. This type of stress relief via oxide's creeping can be experimentally confirmed by the ridge character of Y-doped oxide film in Fig. 3(b). Detailed studies of internal residual stress of oxide films measured by laser Raman spectrum on Y-implanted Co-40Cr and Y-implanted nickel were reported in Refs. [4] and [6].

During the isothermal oxidizing stage, the growth stress σ_{gw} is caused by volume change when the metal is oxidized to its oxide, which can be quantitatively correlated to Pilling-Bedworth ratio (PBR) (volume of oxide/ volume of metal consumed). For chromium, this value is 1.57 and the internal growth stress within the Cr_2O_3 oxide film is compressive[2]. At the air-cooling stage, thermal stress is generated due to the linear thermal expansion difference between Cr_2O_3 and the substrate metal. This thermal stress σ_{th} is also compressive and can be expressed as

$$\sigma_{th} = \frac{E_{OX}\Delta T(\alpha_M - \alpha_{OX})}{1 - \nu}, \qquad (2)$$

where E_{OX} is the Young's modulus of the oxide, ν is the Poisson's ratio of the oxide. α_M and α_{OX} are the thermal expansion coefficients of the metal and oxide, respectively, and ΔT is the temperature change. So the total compressive stress σ_{OX} in the oxide film can be expressed as

$$\sigma_{OX} = \sigma_{gw} + \frac{E_{OX}\Delta T(\alpha_M - \alpha_{OX})}{1 - \nu}. \qquad (3)$$

When the accumulated compressive stress σ_{OX} in the oxide film reached a critical value, cracking and spalling will occur inside the film with the critical stress σ_C and σ_S for cracking and spalling, respectively. In most cases, the first term in the right hand side of Eq. (3) is much smaller than the second term, and can be omitted[2]. This can also be experimentally confirmed by acoustic emission test shown in Fig. 4 that rare AE signal is detected at the 90 h isothermal oxidizing stage and lots of AE signals are detected at the air-cooling stage.

The number of AE signals detected at the oxidizing stage and air-cooling stage can be expressed in a function of temperature change as $n = f(\Delta T)$, where n is the number of AE signals collected in a given time interval. According to Zhang's simplification[5], the spalling of oxide above one interfacial defect can generate Z AE events, of which $Z - 1$ from through-thickness cracking along the perimeter of the buckled oxide and 1 from the final spalling, and usually Z is an integer between 5 and 8. Then the number of interfacial defects in a given ΔT interval can be expressed as

$$N = \frac{n}{Z} = \frac{f(\Delta T)}{Z}. \qquad (4)$$

According to Evans[1], the oxide film spalling

process should be preceded by film buckling process above an interfacial defect. When the accumulative compressive stress inside the oxide film reaches a critical value, oxide film buckling will occur above the interfacial defects. The compressive stress in the buckled region is partially released, while the concentrated stress at the perimeter of this region will cause propagation of crack tip towards the outer face of oxide film, and finally result in through-thickness cracking and spalling of oxide film. The critical stress condition can be expressed as

$$\sigma_{OX} = \frac{3.6H^2E_{OX}^2}{C^2}. \quad (5)$$

In this equation, H is the thickness of the oxide film and C is the radius of the interfacial defect (i.e. radius of the local spalled region). This equation implies that each interfacial defect with different radius will spall under different compressive stress level. Since compressive thermal stress is accumulated gradually in the oxide film with the increasing ΔT drop during the air-cooling stage, local oxide upon large interfacial defect will crack and spall at small ΔT drop, while oxide upon small interfacial defect will crack and spall at large ΔT drop, this can also be experimentally confirmed from the AE signal spectrum as shown in Fig.4.

By combining Eqs.(3), (4) and (5) and omitting σ_{gw}, we can get

$$C = 1.9H\left(\frac{E_{OX}(1-\nu)}{\Delta T(\alpha_M - \alpha_{OX})}\right)^{1/2}, \quad (6)$$

$$N = \frac{1}{Z}f\left(3.6\frac{E_{OX}H^2(1-\nu)}{C^2(\alpha_M - \alpha_{OX})}\right). \quad (7)$$

Here, the Young's modulus E_{OX} and Poisson's ratio ν for Cr_2O_3 oxide are 153 GPa and 0.32, respectively; the liner thermal expansion coefficients α_M and α_{OX} for Co-40Cr and Cr_2O_3 are 0.14 K^{-1} and 0.026 K^{-1}, respectively[6,7] (all the above data were averagely taken at 750 ℃). The thickness of Cr_2O_3 oxide films after 90 h isothermal oxidation can be calculated from the mass-gain curves shown in Fig. 2, and Z is taken as integer 6 in our oxide fracture model.

By converting the measured distribution of AE signals in time domain to temperature domain using Hi-Draw2. 1 software in AE-100 acoustic emission apparatus, and by differential calculation of the number of AE signals in temperature domain using Eqs. (6) and (7), we can finally get the interfacial defect number distribution (N) versus defect size (i.e. radius C) as shown in Fig.6.

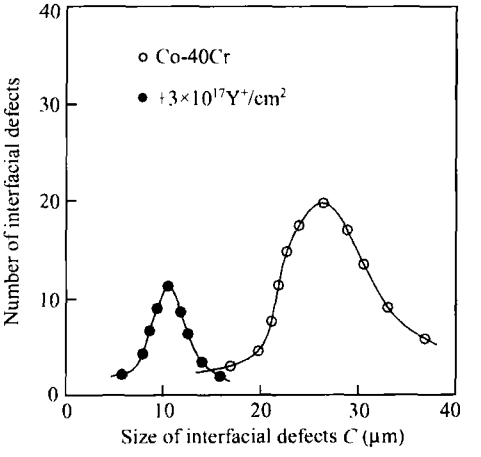

Fig. 6. Number distribution of interfacial defects versus defect sizes.

Fig.6 shows that the interfacial defects' number distribution versus defect size is roughly consistent with Gauss' distribution, and the average interfacial defect radius for Co-40Cr and Y-implanted Co-40Cr are 27.0 μm and 10.5 μm, respectively. Meanwhile, yttrium ion-implantation greatly reduces the total number of interfacial defects, which can be seen by comparing the areas under the two distributional curves in Fig.6.

Fig.7 is the SEM surface morphologies of Cr_2O_3 oxide films formed on Co-40Cr and Y-implanted Co-40Cr after 90 h isothermal oxidation. It can be seen that severe spallation occurs in oxide film formed on Co-40Cr in Fig. 7(a), while few spalled region is found in oxide film formed on Y-implanted Co-40Cr in Fig. 7(b).

The reasons for the improved property of Cr_2O_3 film in anti-cracking and anti-spallation caused by yttrium ion-implantation can be explained in two aspects. Firstly, yttrium ion-implantation can reduce the internal compressive stress and increase the high temperature plasticity of the Cr_2O_3 film. Secondly, yttrium ion-implantation can remarkably reduce the number and size of interfacial defects (Fig. 6) and greatly improve the Cr_2O_3/Co-40Cr interfacial adhesive property. Statistic examination of the size of about 100 spalled areas of Y-free and Y-containing Cr_2O_3 oxide films in our experiment by SEM method indicates that the average defect size tested by acoustic emission method is about 1.5—2.0 times larger

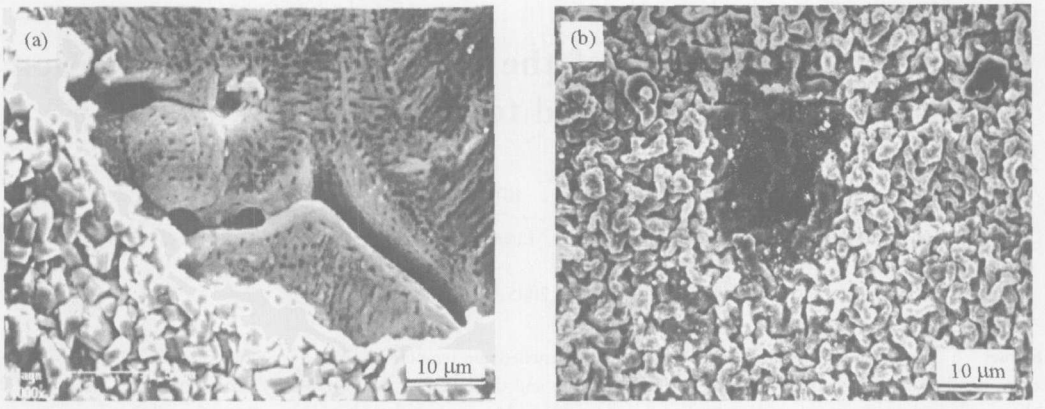

Fig. 7. SEM morphologies of oxide films formed on (a) Co-40Cr and (b) Y-implanted Co-40Cr after 90 h isothermal oxidation.

than the SEM-observed average size of the spalled regions. The reason for higher AE-tested value of defect size is probably due to the interaction between near existing defects, for the stress relief of one defect will have great influence on the near-located defects' stress status. Przybilla[7] has studied the overall mechanical behavior of near-located interfacial defects by related mathematical method, but the drawback of his "composite defect" model is that in real cases the oxide films upon these interfacial defects with different sizes do not crack or spall at the same time but one after another. In addition, the choosing of such values as Young's modulus, Poisson's ratio and thermal expansion coefficient of oxide film with different microstructures at different temperatures may be another reason for the higher AE-tested average defect size in our experiment.

Although it is difficult to propose very accurate mechanical models to study the cracking and spalling of oxide films with different microstructures, acoustic emission method still has apparent advantages and has been used by some researchers[5,8]. Further detailed investigations on this promising method are still needed and must be combined with other oxidation research methods.

4 Conclusion

(i) Yttrium ion-implantation can remarkably reduce the isothermal oxidizing rate of Co-40Cr at 1000 ℃. Meanwhile, the anti-cracking and anti-spalling properties of the Cr_2O_3 oxide film can be much improved by yttrium ion-implantation. Effects of these rare earth are mainly attributed to the lower internal stress level, the grain size refining effect and the improved high temperature plasticity and creeping property of Cr_2O_3 oxide film.

(ii) Yttrium ion-implantation can reduce the number and size of oxide/substrate interfacial defects and improve the adhesive property of oxide film. By using proper mechanical and mathematical methods to simulate the fracture process of oxide film, acoustic emission seems to be a promising method for quantitatively examining the oxide/substrate interfacial behaviors.

References

1 Evans A. G. and Cannon R. Stress and decohesion of oxide scales. Materials Science Forum, 1989, 43(3): 243—265.
2 Rahmel A. and Schutze M. Mechanical aspects of rare earth effects. Oxidation of Metals, 1992, 38(2): 314—328.
3 Jin H. M., Li T. F., Li M. S. et al. Influence of yttrium implantation on oxidation behavior of Co-40Cr alloy. Journal of Rare Earths, 1999, 17(1): 34—38.
4 Jin H. M., Zhang J. F., Yan K. et al. Rare earth effects on high temperature oxidation of pure nickel at 1000 ℃. Progress in Natural Science, 2004, 14(4): 373—377.
5 Zhang Y. F., Shores D., Rahmel A. et al. Spallation of oxide scales formed on Ni-30Cr alloy. Oxidation of Metals, 1993, 40(1): 529—535.
6 Jin H. M., Zhang L. N., Li M. S. et al. Rare earth effects on adhesion of Cr_2O_3 oxide scale formed on surface of Co-40Cr alloy. Journal of Rare Earths, 2001, 19(1): 34—39.
7 Przybilla W. and Schutze M. Role of growth stresses on the structure of oxide scales on nickel at 800 and 900 ℃. Oxidation of Metals, 2002, 58(1): 103—120.
8 Ul-Hamid A. Study of the effect of Y on the scale microstructures of Cr_2O_3- and Al_2O_3-forming alloys. Oxidation of Metals, 2002, 58(1): 23—46.